



OPEN ACCESS

EDITED BY
Caijun Xu,
Wuhan University, China

REVIEWED BY
Kaihua Ding,
China University of Geosciences
Wuhan, China
Xuhua Shi,
Zhejiang University, China
Ming Hao,
The Second Monitoring and Application
Center, China Earthquake
Administration, China

*CORRESPONDENCE

Kaiying Wang,
wangky@aies.ac.cn

SPECIALTY SECTION

This article was submitted to Structural
Geology and Tectonics,
a section of the journal
Frontiers in Earth Science

RECEIVED 23 June 2022
ACCEPTED 24 August 2022
PUBLISHED 15 September 2022

CITATION

Wang K and Feng X (2022), Crustal
deformation and dynamics of the
south-eastern tibetan plateau from
stress fields and geodesy.
Front. Earth Sci. 10:976380.
doi: 10.3389/feart.2022.976380

COPYRIGHT

© 2022 Wang and Feng. This is an open-
access article distributed under the
terms of the [Creative Commons
Attribution License \(CC BY\)](https://creativecommons.org/licenses/by/4.0/). The use,
distribution or reproduction in other
forums is permitted, provided the
original author(s) and the copyright
owner(s) are credited and that the
original publication in this journal is
cited, in accordance with accepted
academic practice. No use, distribution
or reproduction is permitted which does
not comply with these terms.

Crustal deformation and dynamics of the south-eastern tibetan plateau from stress fields and geodesy

Kaiying Wang^{1*} and Xiangdong Feng²

¹State Key Laboratory of Earthquake Dynamics, Institute of Geology, Beijing, China, ²Hebei Earthquake Agency, Shijiazhuang, China

South-eastern Tibet rotates clockwise around the eastern Himalayan syntaxis due to the eastward extrusion of the eastern Tibetan lithosphere and it attracts much attention as a window for studying the dynamics of continental collision between India and Eurasia. Competing geodynamic models to describe the deformation of the eastern Tibet have been the debating subject and the dynamic processes responsible for plateau evolution remain poorly understood, partly because the mechanical state at depth and its relationship with surficial deformation are unclear. In this context, a continuous east-west oriented tensional zone was identified at the south-eastern edge of the Tibetan Plateau based on seismogenic stress field and global positioning system data. The profiles of surficial velocity field reveal a relatively speedy motion belt parallel to the Xianshuihe fault extending from north to south in the rotating region east of the tensional zone. Segmented features of the profiles around the extensional zone indicate its close relation with flow channels delineated from magnetotelluric images. Therefore, the deformation at the south-eastern edge of the Tibetan Plateau is mechanically coupled within the crustal depth. We propose a complex regional kinematics with a localised speedy belt and a continuously extensional zone, where material coupling and deformation compatibility were revealed within the crustal depth.

KEYWORDS

south-eastern Tibetan plateau, focal mechanism, stress field, global positioning system, surface velocity field

Introduction

The India-Eurasia collision has been well established to provide a critical control on the present-day crustal stress field and tectonic deformation in the Tibetan Plateau and its surrounding region. As a result of post-collisional convergence, south-eastern Tibet rotates clockwise around the eastern Himalayan syntaxis (Burchfiel et al., 1995; Chen et al., 2000; England and Houseman, 1986; Royden et al., 1997; Tapponnier and Molnar, 1976; Tapponnier et al., 1982; Wang et al., 1998; Wang and Shen, 2020) due to the eastward extrusion of the lower crustal materials from the plateau, obstruction by the

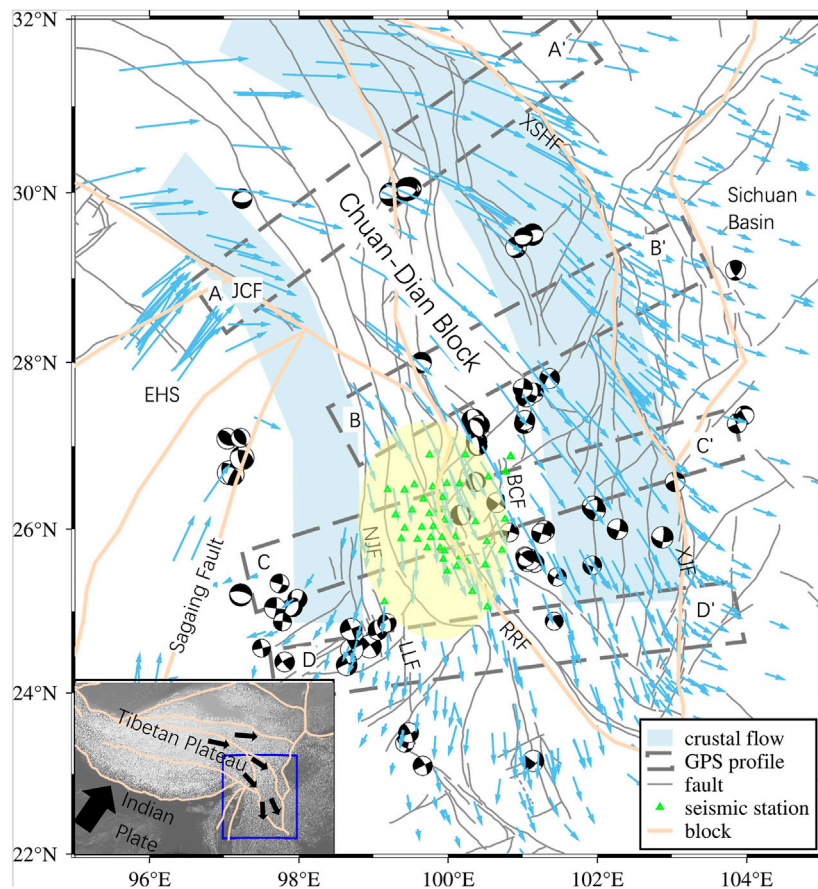


FIGURE 1

Topographic map of south-eastern Tibet. Focal mechanism (1976–2010): from the global CMT catalogue; blue arrows: GPS velocity field relative to Eurasian Plate (Wang and Shen, 2020); Light blue polygons represent crustal flow channels delineated using magnetotelluric data (Bai et al., 2010). The yellow area represents the extensional zone based on focal mechanism and GPS analysis; Black arrows show regional crustal motions. NJF = Nujiang Fault; LLF = Longling Fault; BCF = Binchuan Fault; RRF = Red-River Fault; XSHF = Xianshuihe Fault; XJF = Xiaojiang Fault; JCF = Jiali-Chayu Fault; and EHS = eastern Himalayan syntaxis.

Sichuan Basin (which appears to be deeply rooted and mechanically strong), and certain materials turning southward. The clockwise rotation can be deduced from the distribution of global positioning system (GPS) movement rates (Zhang et al., 2004; Wang and Shen, 2020), major fault slip rates, such as 9–12 mm sinistral slip rates along the Xianshuihe-Xiaojiang fault system (Xu et al., 2003; Wang et al., 2009; Gan et al., 2021), and sinistral coseismic rupture of large earthquakes along the major fault (Figure 1).

The deformation and dynamics of the south-eastern edge of the Tibetan Plateau are important for understanding continent collision where a part of the plateau material is extruded. Several geophysical observation studies in south-eastern Tibet have suggested that low-velocity or mechanically weak zones exist in the mid-lower crust and indicate the possibility of crustal flow

(Bai et al., 2010; Bao et al., 2015; Chen et al., 2016; Fu et al., 2010; Li et al., 2008; Liu et al., 2014; Xu and Song, 2010; Yao et al., 2010; Zhao et al., 2013). Although the existence of weak lower crust and probable crustal flow in south-east (SE) Tibet has attracted significant attention, the mechanism remains enigmatic in determining how the crustal material structure, including a weak lower crust, influences the crustal deformation and how the tectonic stress field links dynamics between the surficial and deep deformations. Mid-crustal deformation is not directly constrained by surficial measurements, and the motion may be different from that observed at the surface, considering the coupling of crustal materials at different depths.

In 2018, our dense digital seismic network (30 stations) with a sampling rate of 100 Hz, was deployed within a $2^{\circ} \times 2^{\circ}$ area near the middle of the Sichuan-Yunnan block, which is bounded by

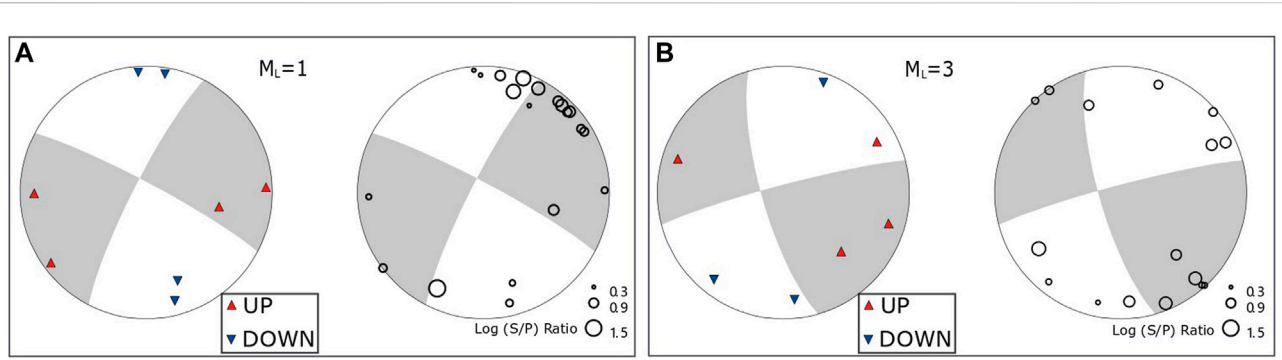


FIGURE 2
Two focal mechanism cases based on P-wave polarities and S/P ratios.

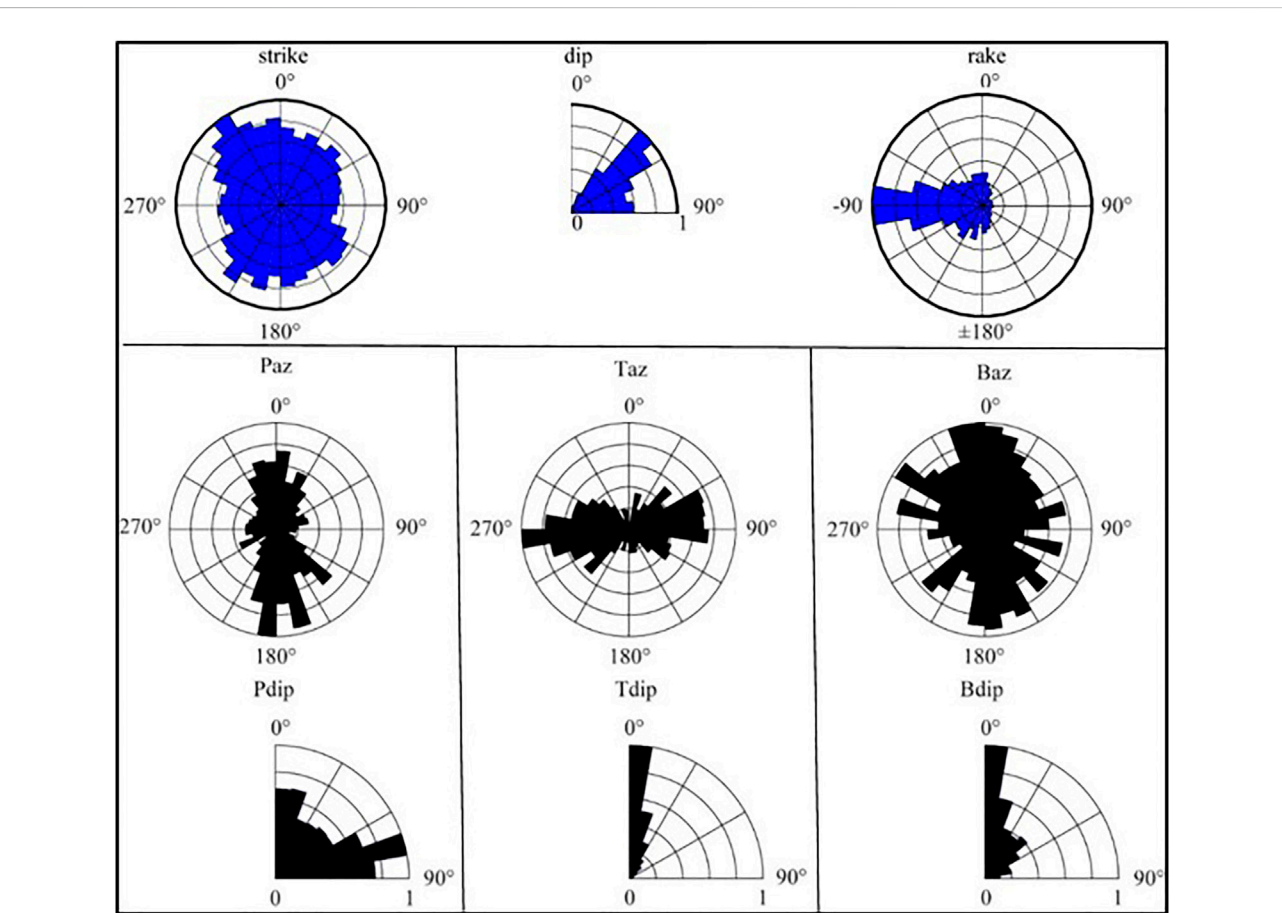


FIGURE 3
Wind rose map showing nodal planes and three focal mechanism axes. The top line shows strikes, dip angles and rakes of the focal mechanisms, and three columns below show azimuths and dip angles for three axes including P, T and B.

the Red-River and Xianshuihe-Xiaojiang faults. Adding some regional permanent stations, the network (Figure 1) recorded over 20,000 earthquakes with M_L 1.3–4.6 between April 2018 and

December 2020. In this study, we examined the deep stresses after determining focal mechanisms based on these events and investigated surficial deformation using GPS velocity data.

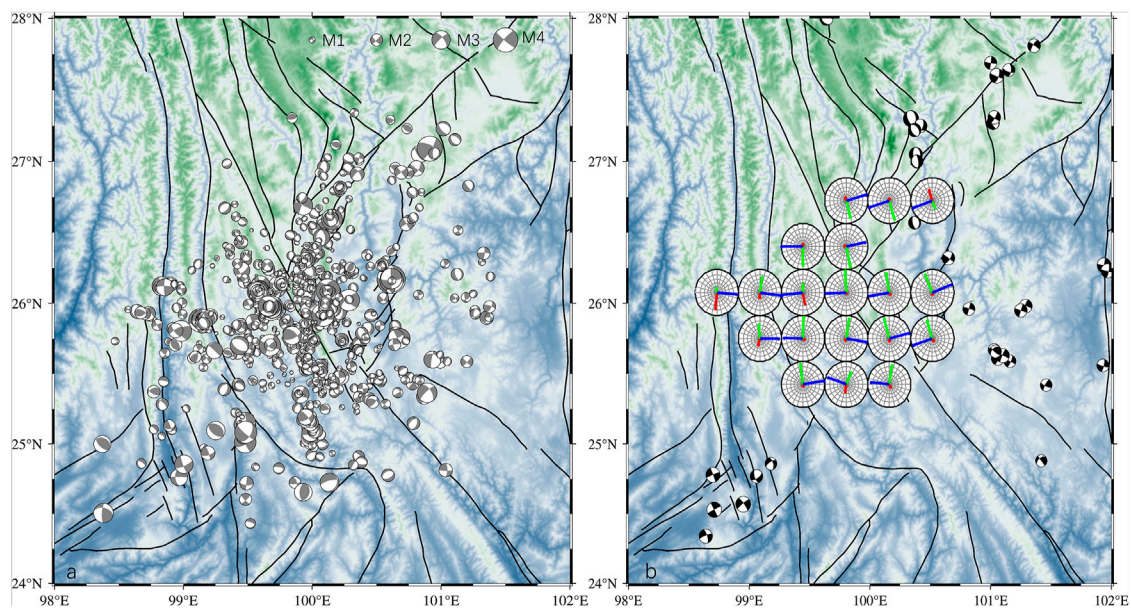


FIGURE 4

(A) Distribution of focal mechanisms based on seismic events recorded by the digital stations shown in Figure 1. (B) Projections on the horizontal plane of the three principal stress axes inverted from the focal mechanisms displayed in (A), including the maximum principal stress axes σ_1 (red), medium principal stress axes σ_2 (green), and minimum principal stress axes σ_3 (blue). The background focal mechanisms are from the global CMT catalogue for events with magnitudes above 5.

Focal mechanisms and stress field

The estimation of the stress field by focal mechanisms is an effective tool for understanding crustal mechanics. Focal mechanisms of small earthquakes are generally determined from P-wave first-motion polarities, and the solutions are extremely sensitive to various errors, including inadequate knowledge about the seismic velocity structure. Many studies added S/P amplitude ratios to constrain focal mechanisms as P-wave amplitudes are larger near the P and T axes of the focal mechanism and smaller near the nodal planes (Kisslinger, 1980; Ruy-Juin [Rau et al., 1996](#); [Snoko, 2003](#)). In this study, we used the HASH method ([Hardebeck, 2002](#); [Hardebeck and Shearer, 2003](#)), which was developed to produce stable focal mechanisms considering the various sources of uncertainty based on P-wave first-motion polarities combining S/P amplitude ratios.

After manually measuring P-wave first-motion polarities and S/P amplitude ratios and using the regional three-dimensional velocity structure data ([Yang et al., 2020](#)), we obtained 1,500 focal mechanism solutions for events with a quality grade above C from the five classes of acceptable mechanisms using the quality criteria based on the solution stability ([Figure 2](#); [Supplementary Table S1](#)).

We performed a statistical analysis of relevant parameters for the focal mechanism solutions ([Figure 3](#)). The wind rose maps of two groups of nodal planes depict an even distribution for strikes

and normal faulting with high dip angles. North-south (NS)-oriented P axes with high dip angles and horizontal east-west (EW)-oriented T axes are dominant for these focal mechanisms.

Subsequently, we used the mature software package MSATSI ([Hardebeck and Michael, 2006](#); [Martinez-Garzon et al., 2014](#)) to invert the stress orientations from the focal mechanisms. The data were divided into 30 grid points that vary by latitude and longitude over the study area. Each grid containing at least 15 focal mechanisms was allowed to invert three principal stress axes ([Figure 4](#)).

The principal stress axes ([Figure 4B](#)) are depicted as projections onto the horizontal plane; therefore, large dip angles corresponded to short axes. The stress field distribution shows that the maximum principal stress axes σ_1 are consistently vertical, the intermediate principal stress axes σ_2 are N-S oriented, and the minimum principal stress axes σ_3 are approximately horizontal with an EW-orientation, demonstrating that the covering area is under a continuously EW-oriented extensional crustal stress environment. Focal mechanisms of mid-large earthquakes from the United States Geological Survey around the area also show normal faulting primarily along a series of NS-oriented arc faults near the east boundary of our study area, such as the Binchuan Fault. The extensional deformation of the area was noticed previously and $\sim 3 \times 10^{-8} \text{ yr}^{-1}$ E-W extension was estimated from GPS data in the region which was explained by gravity-driven deformation using

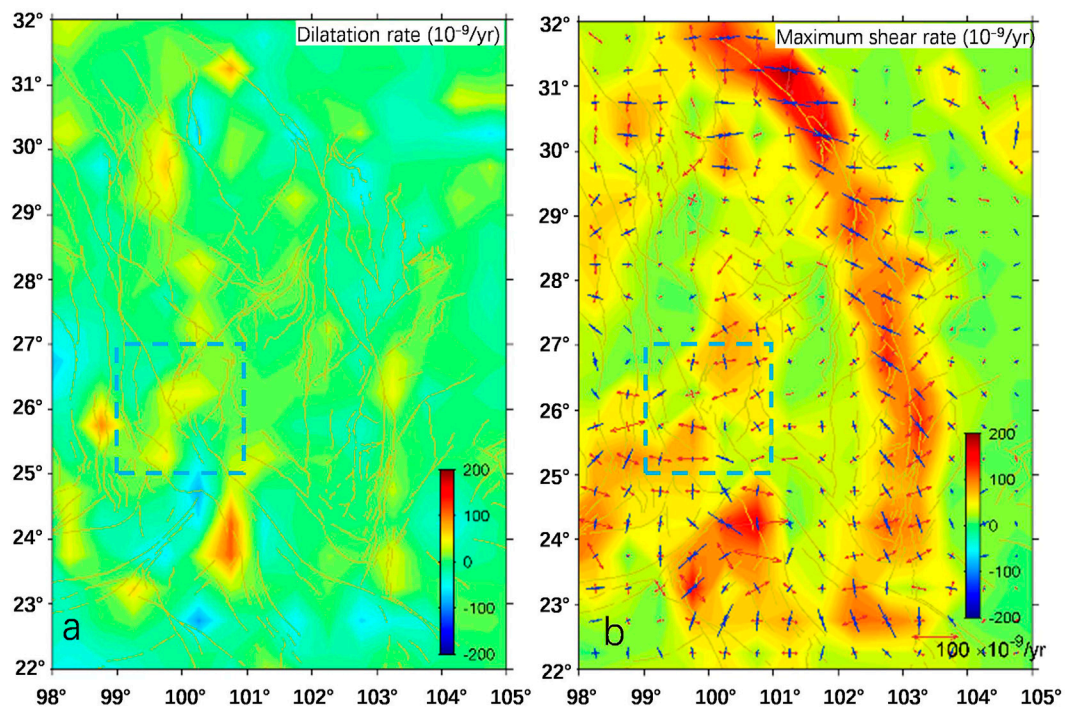


FIGURE 5

Continuum deformation field of Chuan-Dian area derived from interpolation of GPS velocities. Blue dotted square denotes the extensional area in Figure 4. (A) Dilatation rate, with extension positive. (B) Strain rates. Maximum shear strain rate is shown in background colour and principal strain rates are shown as vector pairs.

numerical simulation (Copley, 2008). To the south-west and south-east, the focal mechanisms show NE- and NW-oriented P axes, respectively. The above mechanical frame revealed that the extensional area was stretched toward both side terranes, and the eastern boundary should be delimited by the normal faults of the arc.

Analysis of GPS data

To visualize the crustal deformation field in the study area, we interpolated the GPS velocity data with respect to the Eurasian Plate during the past 25 years (Wang and Shen, 2020) using the “griddata” function of MATLAB, and utilized the expressions in spherical coordinates developed by Savage et al. (2001) to calculate strain rates. The derived GPS strain rates of Chuan-Dian area and the dilatational strain (Figure 5A) accorded with the extensional area resulted from stress inversion, where principle strain axes (Figure 5B) also revealed E-W extension.

We selected several profiles (Figure 1) perpendicular to the strike of the XSH-XJ fault to explore lateral variances of deformation in the clockwise rotating region. Velocity distributions in four profiles (Figure 6A) reveal a relatively

speedy belt that covers segments with longitudes from 99.7°E to 101.5°E for A–A′, 100.2°E to 102°E for B–B′, 101.1°E to 102.7°E for C–C′, and 101.5°E to 102.8°E for D–D′, respectively. From the profiles, the belt is shown to be parallel to the Xianshuihe–Xiaojiang Fault, extending from north to south within the Sichuan–Yunnan block. Notably, the belt location is consistent with the eastern flow channel of the two in SE Tibet (Figure 1), which is approximately 200 km wide with a depth of 20–40 km, as found by Bai et al. (2010) based on their magnetotelluric survey, extending from SE Tibet into south-west China.

Based on the southward surficial movement, we use the E-W components of GPS velocities along the four profiles (Figure 6B) to describe relative movements across the clockwise rotating terrane in the SE plateau. A general feature of the E-W velocity profiles is still reflecting the same speedy belt as that of the velocity profiles. Another feature is that the E-W velocities of the profiles reveal evident segmentation, and the western and eastern areas on the two sides of the extensional zone move outward. For the profiles of B–B′, C–C′ and D–D′ in details, which cover the extensional area, three segments at different E-W rates are separated respectively by the Nujiang–Longling faults and the Binchuan fault along the western and eastern boundaries of the extensional area. The western segments of the profiles exhibit westward movement, and the eastern segments

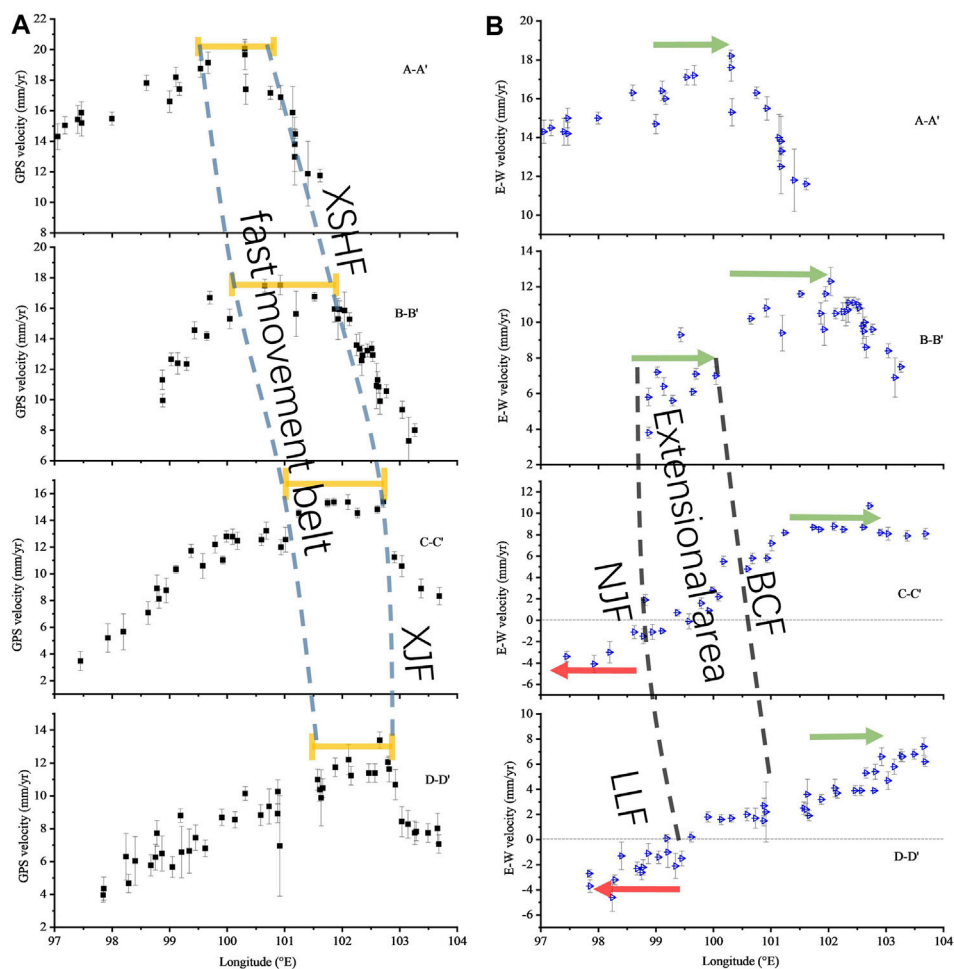


FIGURE 6

(A) GPS velocities in the four profiles shown in Figure 1. The orange line segments mark the comparatively high velocities, and two dashed lines define the fast movement belt; (B) GPS EW velocities in the profiles. The green arrows represent the eastward velocities, and the red ones represent the westward velocities. Two black dashed lines define the extensional area from our study. NJF = Nujiang Fault; LLF = Longling Fault; BCF = Binchuan Fault; RRF = Red-River Fault; XSHF = Xianshuihe Fault; and XJF = Xiaojiang Fault.

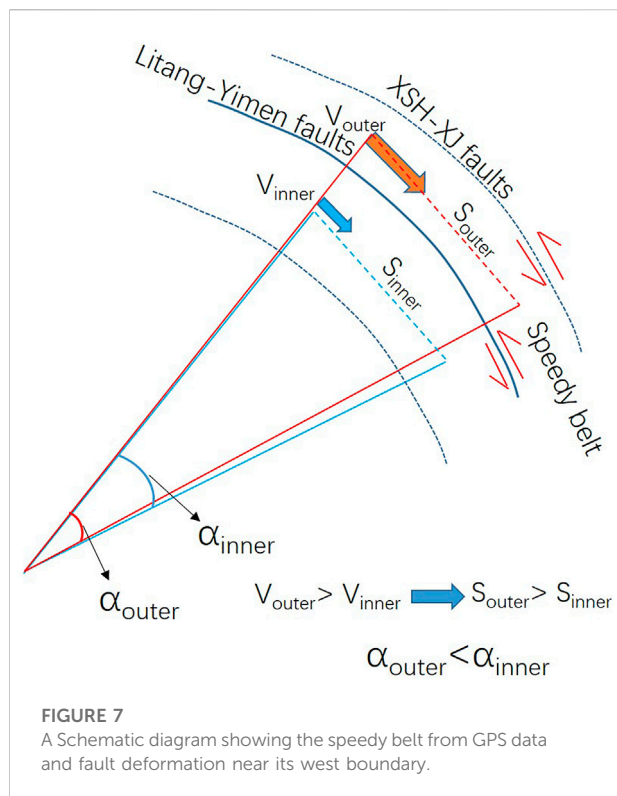
exhibit eastward movement; therefore, the middle terrane between them must have been stretched outward. The other flow channel with high electrical conductivity in SE Tibet (Bai et al., 2010) is located along the western segments of the profiles. Combined with the above stress field, the GPS E-W velocity profiles outline the range of the extensional zone, taking the Nujiang-Longling fault system and the Binchuan fault as western and eastern boundaries, respectively.

Discussion

“Contradictory” mode of fault slip near west boundary of the speedy belt

The analysis of the GPS profiles in this study shows that there is a special belt on the west side of the XSH fault, which should be

understood from different perspectives. The premise of treating it as a speedy belt is that the Chuan-Dian block in the west of the XSH-XJ fault is mainly characterized by translational motion with small strain within several decades, and distribution of movement rates in each profile show peak segment within the belt. On the other hand, according to rotation rate distribution relative to the stable Eurasia plate (Wang and Shen, 2020), this belt is gradient located in the transforming zone from clockwise rotation of the Chuan-Dian block to counterclockwise rotation of the XSH-XJ fault. On the west of the belt, the GPS velocities show linear increase from west to east along the profile strikes, which can be regarded as “uniform motion” with constant angular velocity ($v=\omega r$) in the area, and shortage of several mm/yr within the belt is revealed from the velocity profiles. Geological ages of accumulation reflected that faults in between behaved left lateral as sketched in Figure 7, which seems to “contradict” our



understanding of fault deformation near the west boundary of the speedy belt but accords with the fact that a series of faults from north to south in the Chuan-Dian block near the west boundary of the belt (such as Litang fault, Yimen fault, etc) showed left-lateral slip (Wang et al., 1998).

Results of previous studies (Chen et al., 2014; Bao et al., 2015; Chen et al., 2016; Liu et al., 2021) on the Low-velocity zone revealed different locations of channel flows or highly disconnected and heterogeneous of the low velocity zones beneath the Chuan-Dian block, reflecting large uncertainties of geophysical results in this region. A 3D geo-electrical model from SINOPROBE MT (Dong et al., 2016), located to NW of the Chuan-Dian block area, proposed that “extensional extrusion” mechanism of the south-eastward expansion of Tibetan Plateau may result from the accumulated east-west spreading of a series of local ductile extensions zones.

The extensional area determined from our stress field inversion and GPS deformation revealed a consistent deformation pattern from surface to seismogenic depth. The coupling state between deep and shallow materials in the tensional area may be representative in the Chuan-Dian block. Based on the diversity of geophysical observations, the surficial speedy belt and the east possible crustal channel with high conductivity at the same location revealed similar coupling deformation, revealing that the region deforms by a more complex pattern. This pattern is influenced by localised low velocity zones than typical models suggested, wherein the

plateau may deform through the movements of rigid crustal blocks along large strike-slip faults (Tapponnier and Molnar, 1976; Tapponnier et al., 1982), by continuous deformation (Houseman and England, 1993; Holt et al., 2000) or by crustal flow (Royden et al., 1997; Clark and Royden, 2000).

Seismic anisotropy (Sol et al., 2007) determined using shear-wave splitting analysis revealed a sharp change in the orientation of fast directions from NS in the north to EW in the south of our extensional zone, suggesting that EW strain was mechanically coupled across the crust–mantle interface and strong lower crust to transmit stress. So the coupling state of consistent deformation from shallow to depth may reach the crust–mantle boundary in this area.

Conclusions

The inverted focal mechanisms and stress field based on waveform data from our seismic network revealed that a continuously EW-oriented extensional zone existed at the edge of the SE plateau, where previous middle earthquakes lying at the east boundary of the zone exhibited normal faulting and EW-oriented extensional mechanisms. Analyses based on GPS data also revealed the EW tensional deformation. From surficial GPS velocities, we also observed a speedy belt located inside the clockwise rotating region around the eastern Himalaya syntaxis which was not previously noticed, and the belt location coincides with a crustal flow channel from the magnetotelluric study. We suggest a complex regional kinematics with a localised speedy belt and a continuously extensional zone, where material coupling and deformation compatibility were revealed within the crustal depth.

Data availability statement

The original contributions presented in the study are included in the article/Supplementary Material, further inquiries can be directed to the corresponding author.

Author contributions

KW analyzed data and wrote the manuscript. XF determined the focal mechanisms.

Acknowledgments

We thank Mingpei Jin, Honghu Ma, Wenjie Dang, and their colleagues for field work and extraction of seismic phases. We thank Peixun Liu, Shunyun Chen, Yanshuang Guo, and Yanqun

Zhuo for giving helpful suggestions. We thank National Nonprofit Fundamental Research Grant of China, Institute of Geology, China Earthquake Administration (grant number IGCEA2210) and the National Key R&D Program of China (grant number 2018YFC1503303) for providing financial supports.

Conflict of interest

The authors declare that the research was conducted in the absence of any commercial or financial relationships that could be construed as a potential conflict of interest.

The reviewer MH declared a shared affiliation with the authors to the handling editor at the time of review.

References

- Bai, D., Unsworth, M. J., Meju, M. A., Ma, X., Teng, J., Kong, X., et al. (2010). Crustal deformation of the eastern Tibetan Plateau revealed by magnetotelluric imaging. *Nat. Geosci.* 3, 358–362. doi:10.1038/ngeo830
- Bao, X., Sun, X., Xu, M., Eaton, D. W., Song, X., Wang, L., et al. (2015). Two crustal low-velocity channels beneath SE Tibet revealed by joint inversion of Rayleigh wave dispersion and receiver functions. *Earth Planet. Sci. Lett.* 415, 16–24. doi:10.1016/j.epsl.2015.01.020
- Burchfiel, B. C., Zhiliang, C., Yupinc, L., and Royden, L. H. (1995). Tectonics of the longmen Shan and adjacent regions, central China. *Int. Geol. Rev.* 37, 661–735. doi:10.1080/00206819509465424
- Chen, H., Zhu, L., and Su, Y. (2016). Low velocity crustal flow and crust-mantle coupling mechanism in Yunnan, SE Tibet, revealed by 3D S-wave velocity and azimuthal anisotropy. *Tectonophysics* 685, 8–20. doi:10.1016/j.tecto.2016.07.007
- Chen, M., Huang, H., Yao, H., van der Hilst, R., and Niu, F. (2014). Low wave speed zones in the crust beneath SE Tibet revealed by ambient noise adjoint tomography. *Geophys. Res. Lett.* 41, 334–340. doi:10.1002/2013GL058476
- Chen, Z., Burchfiel, B. C., Liu, Y., King, R. W., Royden, L. H., Tang, W., et al. (2000). Global Positioning System measurements from eastern Tibet and their implications for India/Eurasia intercontinental deformation. *J. Geophys. Res.* 105, 16215227–16216227. doi:10.1029/2000JB900092
- Clark, M. K., and Royden, L. H. (2000). Topographic ooze: Building the eastern margin of Tibet by lower crustal flow. *Geology* 28, 703–706. doi:10.1130/0091-7613(2000)28<703:TOBTM>2.0.CO;2
- Copley, A. (2008). Kinematics and dynamics of the southeastern margin of the Tibetan Plateau. *Geophys. J. Int.* 174 (3), 1081–1100. doi:10.1111/j.1365-246X.2008.03853.x
- Dong, H., Wei, W., Jin, S., Ye, G., Zhang, L., Jing, J., et al. (2016). Extensional extrusion: Insights into south-eastward expansion of Tibetan Plateau from magnetotelluric array data. *Earth Planet. Sci. Lett.* 454, 78–85. doi:10.1016/j.epsl.2016.07.043
- England, P., and Houseman, G. (1986). Finite strain calculations of continental deformation: 2. Comparison with the India-Asia collision zone. *J. Geophys. Res.* 91, 3664–3676. doi:10.1029/JB091iB03p03664
- Fu, Y. V., Li, A., and Chen, Y. J. (2010). Crustal and upper mantle structure of southeast Tibet from Rayleigh wave tomography. *J. Geophys. Res.* 115, B12323. doi:10.1029/2009JB007160
- Gan, W., Molnar, P., Zhang, P., Xiao, G., Liang, S., Zhang, K., et al. (2021). Initiation of clockwise rotation and eastward transport of Southeastern Tibet inferred from deflected fault traces and GPS observations. *The Geol. Soc. Am. Spec.* 134 (5–6), 1129–1142. doi:10.1130/B36069.1
- Hardebeck, J. L. (2002). A new method for determining first-motion focal mechanisms. *Bull. Seismol. Soc. Am.* 92, 2264–2276. doi:10.1785/0120010200
- Hardebeck, J. L., and Michael, A. J. (2006). Damped regional-scale stress inversions: Methodology and examples for southern California and the Coalinga aftershock sequence. *J. Geophys. Res.* 111 (B11310). doi:10.1029/2005JB004144
- Hardebeck, J. L., and Shearer, P. M. (2003). Using S/P amplitude ratios to constrain the focal mechanisms of small earthquakes. *Bull. Seismol. Soc. Am.* 93, 2434–2444. doi:10.1785/0120020236
- Holt, W. E., Chamot-Rooke, N., Pichon, X. L., Haines, A. J., Shen-Tu, B., and Ren, J. (2000). Velocity field in Asia inferred from Quaternary fault slip rates and global positioning system observations. *J. Geophys. Res.* 105, 19185–19209. doi:10.1029/2000JB900045
- Houseman, G., and England, P. (1993). Crustal thickening versus lateral expulsion in the Indian-Asian continental collision. *J. Geophys. Res.* 98, 12233–12249. doi:10.1029/93JB00443
- Kisslinger, C. (1980). Evaluation of S to P amplitude ratios for determining focal mechanisms from regional network observations. *Bull. Seismol. Soc. Am.* 70, 999–1041. doi:10.1785/BSSA0700040999
- Li, Y., Wu, Q., Zhang, R., Tian, X., and Zeng, R. (2008). The crust and upper mantle structure beneath Yunnan from joint inversion of receiver functions and Rayleigh wave dispersion data. *Phys. Earth Planet. Interiors* 170, 134–146. doi:10.1016/j.pepi.2008.08.006
- Liu, Q. Y., van der Hilst, R. D., Li, Y., Yao, H. J., Chen, J. H., Guo, B., et al. (2014). Eastward expansion of the Tibetan Plateau by crustal flow and strain partitioning across faults. *Nat. Geosci.* 7, 361–365. doi:10.1038/ngeo2130
- Liu, Y., Yao, H., Zhang, H., and Fang, H. (2021). The community velocity model V.1.0 of southwest China, constructed from joint body- and surface-wave travel-time tomography. *Seismol. Res. Lett.* 92, 2972–2987. doi:10.1785/0220200318
- Martinez-Garzon, P., Kwiatek, G., Ickrath, M., and Bohnhoff, M. (2014). MSATSI: A MATLAB package for stress inversion combining solid classic methodology, a new simplified user-handling, and a visualization tool. *Seismol. Res. Lett.* 85, 896–904. doi:10.1785/0220130189
- Rau, R. J., Wu, F. T., and Shin, T. C. (1996). Regional network focal mechanism determination using 3D velocity model and SH/P amplitude ratio. *Bull. Seismol. Soc. Am.* 86, 1270–1283.
- Royden, L. H., Burchfiel, B. C., King, R. W., Wang, E., Chen, Z., Shen, F., et al. (1997). Surface deformation and lower crustal flow in Eastern Tibet. *Science* 276, 788–790. doi:10.1126/science.276.5313.788
- Savage, J. C., Gan, W., and Svarc, J. (2001). Strain accumulation and rotation in the eastern California sheath zone. *J. Geophys. Res.* 106 (21), 109955–B11022.
- Snoko, J. A., 2003. FOCMREC: FOCAL MECHANISM determinations. Available at: <http://www.geol.vt.edu/outreach/vtso/focmec/>. doi:10.1016/S0074-6142(03)80291-7
- Sol, S., Meltzer, A., Bürgmann, R., van der Hilst, R., King, R., Chen, Z., et al. (2007). Geodynamics of the southeastern Tibetan Plateau from seismic anisotropy and geodesy. *Geol.* 35, 563–566. doi:10.1130/G23408A.1
- Tapponnier, P., and Molnar, P. (1976). Slip-line field theory and large-scale continental tectonics. *Nature* 264, 319–324. doi:10.1038/264319a0
- Tapponnier, P., Peltzer, G., Le Dain, A. Y., Armijo, R., and Cobbold, P. (1982). Propagating extrusion tectonics in Asia: New insights from simple experiments with plasticine. *Geol.* 10, 611–616. doi:10.1130/0091-7613(1982)10<611:petian>2.0.co;2
- Wang, E., Burchfiel, B. C., Royden, L. H., Chen, L., Chen, Z., Li, W., et al. (1998). Late cenozoic xianshuihe-xiaojiang, red river, and dali fault systems of southwestern sichuan and central yunnan, China. *Geol. Soc. Am. Spec. Pap.* 327, 1–108. doi:10.1130/0-8137-2327-2.1

Publisher's note

All claims expressed in this article are solely those of the authors and do not necessarily represent those of their affiliated organizations, or those of the publisher, the editors and the reviewers. Any product that may be evaluated in this article, or claim that may be made by its manufacturer, is not guaranteed or endorsed by the publisher.

Supplementary material

The Supplementary Material for this article can be found online at: <https://www.frontiersin.org/articles/10.3389/feart.2022.976380/full#supplementary-material>

- Wang, H., Wright, T. J., and Biggs, J. (2009). Interseismic slip rate of the northwestern Xianshuihe fault from InSAR data. *Geophys. Res. Lett.* 36, L03302. doi:10.1029/2008gl036560
- Wang, M., and Shen, Z. (2020). Present-day crustal deformation of continental China derived from GPS and its tectonic implications. *J. Geophys. Res. Solid Earth* 125, e2019. doi:10.1029/2019JB018774
- Xu, X., Wen, X., Zheng, R., Ma, W., Song, F., and Yu, G. (2003). Pattern of latest tectonic motion and its dynamics for active blocks in Sichuan-Yunnan region. *China. Sci. China (Earth Sci.)*. 46, 210–226. doi:10.1360/03dz0017
- Xu, Z. J., and Song, X. (2010). Joint inversion for crustal and pn velocities and moho depth in eastern margin of the Tibetan plateau. *Tectonophysics* 491, 185–193. doi:10.1016/j.tecto.2009.11.022
- Yang, Y., Yao, H., Wu, H., Zhang, P., and Wang, M. (2020). A new crustal shear-velocity model in Southwest China from joint seismological inversion and its implications for regional crustal dynamics. *Geophys. J. Int.* 220 (2), 1379–1393. doi:10.1093/gji/ggz514
- Yao, H., van der Hilst, R. D., and Montagner, J. (2010). Heterogeneity and anisotropy of the lithosphere of SE Tibet from surface wave array tomography. *J. Geophys. Res.* 115 (B12), B12307. doi:10.1029/2009JB007142
- Zhang, P., Shen, Z., Wang, M., Gan, W., Burgmann, R., Molnar, P., et al. (2004). Continuous deformation of the Tibetan Plateau from global positioning system data. *Geol.* 32, 809–812. doi:10.1130/G20554.1
- Zhao, L., Xie, X., He, J., Tian, X., and Yao, Z. (2013). Crustal flow pattern beneath the Tibetan Plateau constrained by regional Lg-wave Q tomography. *Earth Planet. Sci. Lett.* 383, 113–122. doi:10.1016/j.epsl.2013.09.038